

NUMERICAL STUDIES OF CAHN-HILLIARD EQUATION AND APPLICATIONS IN IMAGE PROCESSING

VLADIMÍR CHALUPECKÝ¹

Abstract. In this article we present a numerical scheme for solving the Cahn-Hilliard equation with degenerate mobility. This scheme is based on the method of lines, we discretize the equation by finite differences in space and the resulting system of ordinary differential equations is solved by an embedded fourth-order Runge-Kutta Cash-Karp method with fifth-order error estimate. The experimental order of convergence suggests that the scheme is accurate of the first order. We also summarize some results concerning the efficiency of parallel implementation. Finally, we consider the application of the scheme for processing of binary images, which contain objects with distorted boundaries, and present various numerical experiments.

Key words. FDM, method of lines, Cahn-Hilliard equation, image processing

AMS subject classifications. 65M06, 65M20, 35K65, 68U10

1. Introduction. The Cahn-Hilliard equation

$$\frac{\partial u}{\partial t} = \nabla \cdot (M(u)\nabla(f'(u) - \gamma\Delta u)), \quad (1.1)$$

has been proposed by Cahn and Hilliard [7, 9] to model isothermal phase separation in binary alloys under critical undercooling. A mixture of two components in a thermal equilibrium is formed by a single phase where both components are present uniformly in the considered domain. After rapid undercooling under the critical temperature the homogeneous state becomes unstable and the system will try to reach the thermal equilibrium. A phase separation will take place and the domain splits into regions rich in one component and poor in the other. Depending on the initial ratio of both components, this process can proceed in two different ways. In the case the mixture contains significantly higher amount of one component, nuclei of the poorer component form and grow. In the case both components are present in basically the same ratio, a process called spinodal decomposition takes place and fine-grained random structures appear and coarsen.

The Cahn-Hilliard equation is a representative of the so-called phase-field models. These arise from a diffuse description of sharp interfaces separating two bulk phases during microstructure processes. The Allen-Cahn equation [8] is another such representative used to model crystalline solidification of a pure liquid. Aside from the modelling of interfacial phenomena, the phase-field equations have recently been successfully applied in the context of image processing. The non-local Allen-Cahn equation and the constant-mobility Cahn-Hilliard equation have been used for shape recovery [11], a modification of the Allen-Cahn equation has been proposed for geometrical image segmentation [5].

¹Department of Mathematics, Faculty of Nuclear Sciences and Physical Engineering, Czech Technical University in Prague, Trojanova 13, 120 00 Prague, Czech Republic.

In this paper we are concerned with a numerical scheme for the degenerate Cahn-Hilliard equation in the following form

$$\frac{\partial u}{\partial t} = \nabla \cdot (M(u)\nabla w), \quad (1.2)$$

$$w = f'(u) - \gamma\Delta u, \quad x \in \Omega, \quad t \in (0, T), \quad (1.3)$$

$$\frac{\partial u}{\partial n} \Big|_{\partial\Omega} = \frac{\partial w}{\partial n} \Big|_{\partial\Omega} = 0, \quad t \in (0, T), \quad (1.4)$$

$$u(x, 0) = u_0(x), \quad x \in \Omega. \quad (1.5)$$

In this fourth-order parabolic equation u represents a relative concentration of one component in a binary mixture, i.e. $u = u_A = 1 - u_B$, $u \in \langle 0, 1 \rangle$, and w denotes a chemical potential. The function $M(u)$ is the degenerate mobility, which restricts diffusion of both components to the interfacial region only. It can be any positive function equal to zero in pure components, in the computations below we use the following form $M(u) = \beta u(1 - u)$, where β is a constant.

The function $f(u)$ is a homogeneous free energy. Mean-field model leads to the form

$$f(u) = \frac{\theta}{2}(u \ln(u) + (1 - u) \ln(1 - u)) + u(1 - u), \quad (1.6)$$

which gives rise to the double-well form for temperatures of undercooling $\theta < 1$. Other forms of the free energy are possible, for instance for $0 \ll \theta < 1$ the function (1.6) can be approximated by

$$f(u) = \frac{1}{4}u^2(1 - u)^2, \quad (1.7)$$

which has the advantage of being smooth.

During the evolution of the initial condition, the domain Ω splits into three different subdomains. Two domains, Ω_0 and Ω_1 , are formed by points where the solution is close to the minima of f (in our formulation 0 and 1) or by points where the binary mixture is rich in one component and poor in the other. The third domain is formed by a thin transition layer, where the solution rapidly changes from 0 to 1. The parameter $\gamma > 0$ is related to the thickness of this interface which is of order $\sqrt{\gamma}$.

Existence of a weak solution for the Cahn-Hilliard equation with degenerate mobility has been proven in [12], there is yet no result concerning the uniqueness.

If the interface width goes to zero, the resulting curve moves according to some geometric motion law. In [10] it has been obtained by method of formal asymptotic expansion that under the scaling

$$t \rightarrow \xi^2 t, \quad \gamma = \xi^2, \quad (1.8)$$

the interface, in the limit $\xi \rightarrow 0$, moves by a geometric motion law called surface diffusion

$$\nu = -\frac{\pi^2}{16}\Delta_s \kappa, \quad (1.9)$$

where ν is the normal velocity of the curve, Δ_s is the Laplace-Bertrami operator and κ is the mean curvature of the interface. This is in contrast to the constant mobility

case, where we get the Mullins-Sekerka problem when $\xi \rightarrow 0$ for the rescaling of time $t \rightarrow \xi t$.

It should also be noted that the integral of the solution of (1.2)–(1.5) is preserved, i.e.

$$\frac{d}{dt} \int_{\Omega} u \, dx = 0.$$

This property of the solution will be important for image processing applications.

2. Numerical scheme. In this section we present a numerical scheme that we propose for the problem (1.2)–(1.5) with the homogeneous free energy in the form (1.7) and with the scaling (1.8). The scheme is based on finite difference discretization in space, the resulting system of ODEs is solved by an embedded fourth-order Runge-Kutta Cash-Karp method with fifth-order error estimate, which enables us to adaptively change the time step [6, 3, 4].

The case of constant diffusive mobility is well investigated and a number of numerical schemes has been proposed based on both finite difference as well as finite element method. In the constant-mobility case, convergence and error estimates are studied, e.g., in [14] for a finite difference scheme in 1-D or in [13] for a mixed finite element scheme in 2- and 3-D. The degenerate-mobility case is more complicated, a finite element method has been proposed in [1, 2], where the convergence (in one space dimension) is studied. A method based on nonlinear multigrid method was proposed in [16].

First, let us present some used notation. By Ω we denote a rectangular computational domain $(0, L_x) \times (0, L_y)$. We discretize the equation on a regular rectangular grid, by $\bar{\omega}_h = \{[ih_x, jh_y] \in \bar{\Omega} \mid i = 0, \dots, m_x - 1; j = 0, \dots, m_y - 1\}$ we denote all grid nodes, by $\omega_h = \{[ih_x, jh_y] \in \bar{\Omega} \mid i = 1, \dots, m_x - 2; j = 1, \dots, m_y - 2\}$ only the inner nodes. The space steps in x , resp. y direction are $h_x = L_x/(m_x - 1)$, $h_y = L_y/(m_y - 1)$, value of function u at the node (i, j) is denoted by $u_{ij} = u(ih_x, jh_y)$.

We look for a solution $u^h = (u_{ij}(t))_{i=0, j=0}^{m_x-1, m_y-1}$ satisfying the following system of ordinary differential equations

$$\frac{du_{ij}}{dt} = \frac{1}{\xi^2} \nabla_h \cdot (M(u^h) \bar{\nabla}_h w)_{ij} \quad \text{on } \bar{\omega}_h, \quad (2.1)$$

where

$$\begin{aligned} \nabla_h \cdot (M(u^h) \bar{\nabla}_h w)_{ij} &= \frac{1}{h_x^2} \left(M(u_{i+1/2j})(w_{i+1j} - w_{ij}) \right. \\ &\quad \left. - M(u_{i-1/2j})(w_{ij} - w_{i-1j}) \right) \\ &\quad + \frac{1}{h_y^2} \left(M(u_{ij+1/2})(w_{ij+1} - w_{ij}) \right. \\ &\quad \left. - M(u_{ij-1/2})(w_{ij} - w_{ij-1}) \right) \quad \text{on } \omega_h, \\ w_{ij} &= f'(u_{ij}) - \xi^2 (\Delta_h u_h)_{ij} \quad \text{on } \omega_h, \\ (\Delta_h u_h)_{ij} &= \frac{1}{h_x^2} (u_{i+1j} - 2u_{ij} + u_{i-1j}) \\ &\quad + \frac{1}{h_y^2} (u_{ij+1} - 2u_{ij} + u_{ij-1}), \end{aligned}$$

and where for instance

$$u_{i+1/2j} = \frac{u_{ij} + u_{i+1j}}{2},$$

Boundary conditions are treated by reflecting u^h at the boundary. For instance

$$u_{-1j} = u_{1j}, \quad j = 0, \dots, m_y - 1,$$

to fulfill the condition $\frac{\partial u}{\partial n}|_{\Gamma} = 0$ and

$$w_{-1j} = w_{1j}, \quad j = 0, \dots, m_y - 1,$$

to fulfill the condition $\frac{\partial w}{\partial n}|_{\Gamma} = 0$.

The system (2.1) is then solved by an embedded fourth-order Runge-Kutta Cash-Karp method with fifth-order error estimate (see e.g. [17]). Since we are using the polynomial approximation of the homogeneous free energy for low undercoolings, the solution is not guaranteed to stay within the interval $(0, 1)$. For stability reasons, we overcome this inconvenience by a heuristical approach where we cut off the solution at each time step.

3. Experimental order of convergence. In this section we demonstrate the experimental order of convergence of our numerical scheme for both the constant-mobility case $M \equiv 1$ as well as for the degenerate-mobility case $M(u) = \beta u(1 - u)$. We measure the convergence by comparing the error between discrete solutions on a set of gradually finer meshes. To compute the error, we use the so-called double-mesh principle [15, 16], where the finer mesh has twice as many grid points in each axis as the coarser mesh.

Our setup for the convergence measurement is as follows. As the initial condition we choose the characteristic function χ_{Λ} of a special set Λ convolved with a smoothing kernel G_{σ} in the following way

$$u_0 = G_{\sigma} * \chi_{\Lambda},$$

$$\Lambda = \{(x, y) \in (0, 1) \times (0, 1) \mid \text{dist}((x, y), 0) > a_1 + a_2 \cos(a_3 \cdot \arctg(y/x))\},$$

where G_{σ} is the Gauss function with the parameter σ small. We compute the solution on uniform grids $h_x = h_y = h_n = 1/(2^n - 1)$, $n = 4, 5, 6, 7, 8, 9$ and we measure the convergence at time $t = 10^{-5}$. This time interval is sufficient for investigating the convergence, the solution changes significantly and the number of time steps for the finest mesh is about $7 \cdot 10^5$. The interface parameter ξ is kept constant in all the computations and is equal to $2/15$, i.e., twice as large as the space step for the coarsest mesh.

To measure the error between two successively finer meshes, we first calculate values of the coarse grid solution at the nodes of the finer mesh by means of bilinear interpolation. We define the error $e_{n,2n}$ to be the discrete L_p norm of the difference of the fine grid solution and the interpolated coarse grid solution. The rate of convergence is then defined as a ratio of successive errors

$$R = \frac{\log(e_{n,2n}) - \log(e_{2n,4n})}{\log(h_n) - \log(h_{2n})}.$$

The results are summarized in Table 3.1 for the case with constant mobility and in Table 3.2 for the degenerate mobility case. In both tables in the first column there

are sizes of the grids between which we measure the error. The error is shown in the corresponding column together with the convergence rate. From Table 3.1 and 3.2 we observe that the scheme converges with first-order accuracy in both the constant as well as the degenerate-mobility case. Theoretical results supporting the observed order of convergence will form a part of author's future work.

Grid sizes	L_2 norm of error	Rate	L_∞ norm of error	Rate
16-32	0.133717	1.164281	0.518882	0.965498
32-64	0.057428	0.940740	0.257440	0.998871
64-128	0.029471	1.029924	0.126778	1.015713
128-256	0.014316	1.053902	0.062201	1.106401
256-512	0.006867		0.028764	

TABLE 3.1

Experimental order of convergence for the Cahn-Hilliard equation with constant mobility

Grid sizes	L_2 norm of error	Rate	L_∞ norm of error	Rate
16-32	0.159477	1.127866	0.694137	1.060878
32-64	0.070326	1.166494	0.321353	1.217638
64-128	0.030751	0.999014	0.135511	0.980905
128-256	0.015265	0.947854	0.068128	0.971427
256-512	0.007884		0.034613	

TABLE 3.2

Experimental order of convergence for the Cahn-Hilliard equation with degenerate mobility

4. Parallel implementation. In order to recover the thin interface layer where the solution changes rapidly, a fine grid has to be used which leads to high computational demands. Therefore, a parallel implementation is a suitable tool to ease the execution of large amount of computational experiments.

We have implemented such a parallel version of the numerical scheme presented in the Section 2 using the MPI standard. We have decided for this distributed-memory environment due to easy availability of cheap clusters of workstations. Moreover, the shared-memory computers we had access to could exploit the parallelism without any changes to the program. Thus, for our purposes we consider the choice of MPI as a parallel environment to be more general than for example OpenMP.

Due to the regular mesh, the implementation is quite straightforward. The computational grid is divided in subdomain and each process is designated one subdomain. During the computation, each process updates only its own subdomain. Values of boundary nodes are computed either from boundary conditions or they are obtained from communication with neighboring processes. All-to-one communication is necessary for I/O operations only and it is kept to minimum.

At this point we should mention that due to the Cash-Karp Runge-Kutta method the amount of communication at one time step increases in the case of shortening the time step and subsequent recomputing the solution. One time step requires six evaluations of the right-hand side and each evaluation requires two communications, one for the solution u and another for the chemical potential w . At early stages of the evolution the algorithm may require to shorten the time step in order to keep the error below a specified threshold and thus the amount of time spent in sending data between processes increases.

Graphs summarizing some preliminary performance results are shown in Figure 4.1 for the case of row-wise division of the computational grid. We realize that this is not ideal, but this is caused by our technical limitations. However, more efficient division by columns and rows has been also implemented.

The parallel speed-up S and efficiency E were measured in the usual way

$$S(P) = T(1)/T(P), \quad E(P) = S(P)/P,$$

where P denotes the number of processors and $T(1)$ and $T(P)$ denote the execution times of the algorithm on one and P processors respectively.

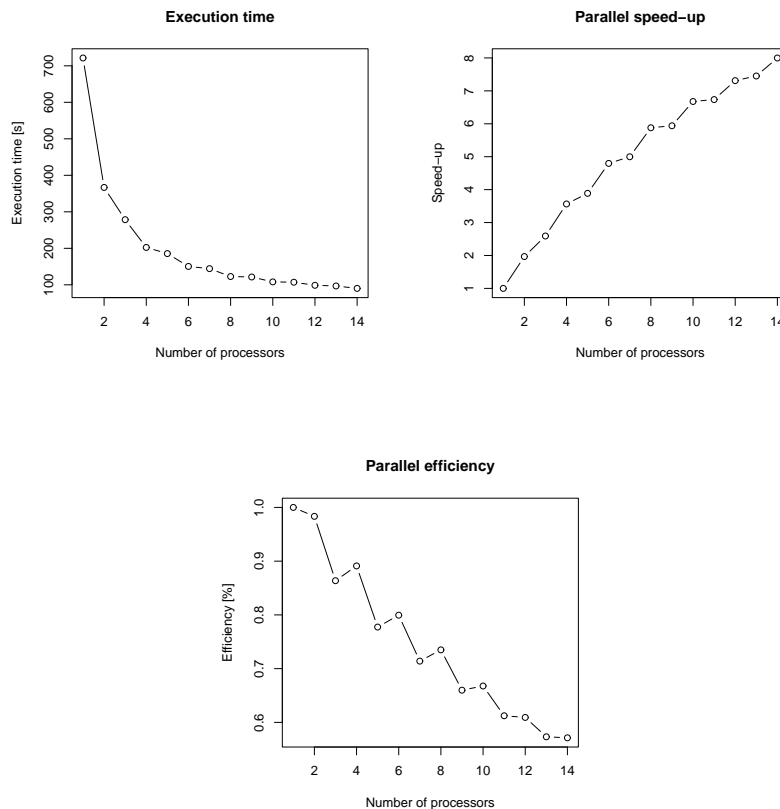


FIG. 4.1. Parallelization: computational grid = 128 × 128 nodes, row-wise distribution of nodes among processes

5. Image processing by the Cahn-Hilliard equation. The image processing applications we consider in this section are concerned with recovering object boundaries in binary images. Such a binary image can be a result of applying some segmentation algorithm on the input image. By image segmentation we mean a process of partitioning an image into regions which are contiguous and relatively homogeneous in image properties (like intensity or texture). Since the real images are almost always degraded by noise, the shapes will not have a smooth boundary which renders any

further processing more difficult. Since good segmentation forms a key step in any image-based recognition system, some preprocessing step is necessary, either at the stage before segmentation or afterwards. The algorithm we consider in this section is meant to be applied on the segmented binary image, where for example zero value of the image function identifies the object in question. In this setting, the object boundary is then identified as those points (pixels) where the image function changes from 0 to 1.

The above described process can be summarized as follows

1. *Image acquisition* – the output of this stage is a gray-scale or color image. This image will be very likely degraded by noise originating either from transmission errors or more often from the limitations of the acquisition technology. A typical example may be a magnetic-resonance imaging scans.
2. *Image preprocessing* – the goal of this stage is to smooth the image while preserving important features in the image. Spurious structures like noise are removed, however, this may happen at the price of smoothing out texture details. These can be an important distinguishing property in the further processing pipeline.
3. *Image segmentation* – at this stage the image domain is divided into contiguous regions of relatively homogeneous image properties. The output is a binary image where for instance the value 0 identifies those points which share the same property of interest. Due to the noise in the original image or due to the natural characteristics of the object, the boundary of these regions will not be smooth. This can make further processing and recognition more difficult.
4. *Shape recovery* – this is the stage that we are concerned about in this section. Its goal is to smooth the noise and small spurious details at the boundaries in the segmented image while preserving important and distinguishing features.

To cope with the task stated in the item 4 of the previous list, we will consider only the boundaries of segmented objects. The noise and spurious details create structures with high curvature. Application of some curvature-dependent motion on the boundaries could smooth out high-curvature details without changing the overall shape of the curve.

In the image processing literature a number of approaches for curve evolution have been proposed (see [11] and references therein). The most often used is the motion by mean curvature

$$\nu = -\kappa, \tag{5.1}$$

where ν denotes the normal velocity of the curve at each point and κ denotes its mean curvature. This motion law is curve-shortening, but it is not area-preserving, a circle moving under this law will shrink to a point in finite time. The original shapes are quickly lost, which implies a necessity for a stopping time.

Consequently, a motion law that is curve-shortening and area-preserving might be more suitable for image processing. These requirements are fulfilled by the so-called *surface diffusion*

$$\nu = -\Delta_s \kappa, \tag{5.2}$$

where ν and κ denote as before the normal velocity of the curve and curvature, respectively, and Δ_s denotes the Laplace-Bertrami operator. This motion law operates on two different scales, which means that small structures on the curve are quickly

smoothed out, while the overall shape changes very slowly in time. We have mentioned in Section 1 that under a suitable scaling that Cahn-Hilliard equation with degenerate mobility asymptotically approximates the surface diffusion. As a result, we propose to apply the Cahn-Hilliard equation with degenerate mobility and its numerical scheme presented in the previous sections in the context of image processing as an algorithm for smoothing and recovering the distorted boundaries of segmented objects. For some numerical experiments, see the following section.

Other choices of area-preserving motion laws for curves are of course possible. The Cahn-Hilliard equation converges for $\xi \rightarrow 0$ to the Mullins-Sekerka problem, the non-local form of the Allen-Cahn equation is area-preserving as well [11].

6. Numerical experiments. In this section we present some numerical experiments using the proposed numerical scheme (2.1) applied to image processing applications.

In all the experiments, the initial condition was chosen as an image resulting from some previous segmentation algorithm. Such an image, represented as a piece-wise constant function defined on the domain Ω and smoothed in the sense of Section 3, can be directly input into the numerical scheme. All the processed image are square, so that the computational domain is always set to $(0, 1) \times (0, 1)$ and the space step is set accordingly to $1/(n-1)$, where n denotes the number of pixels in each dimension. The interface parameter ξ is chosen equal to space step. This choice may not guarantee enough grid points on the interface and therefore the exact recovery of the surface diffusion motion law, but this does not pose a real problem since this is not the goal of the presented image processing application. The constant β was chosen to be equal to $1/4$.

In Figure 6.1 we can see the evolution of an initial shape with four “leaves”, the boundary of which has been damaged by small bumps. The initial condition is in Figure 6.1(a) and the time increases to the right and down. Several images at various times of the evolution are shown, the effect of evolution at two time scales is apparent. The small bumps at the boundary are smoothed out quickly while the overall four-leaf shape almost does not change. Even after a long-time evolution shown in the lower right corner (Figure 6.1(f)) the final shape does not differ much from the original shape.

In Figure 6.2 the processing of a segmented image of a dog is shown. Unlike the previous result, this shape is more complicated and the boundary has been distorted by fine-grained noise. During the evolution this noise is eliminated quickly.

In Figure 6.3 the shape recovery of the letter R is shown. The boundary is again damaged by distorting it by a noise. After a short time of the evolution the noise is smoothed out.

In the last Figure 6.4 the same image of letter R is shown, the only difference from the previous figure being the amount of noise applied to the boundary. Even though the boundary is now quite damaged, after a short time we get result which may be more suitable for further processing.

7. Conclusion. In this paper we have proposed a numerical scheme for solving the Cahn-Hilliard equation with both the constant mobility and the degenerate mobility. This scheme is based on method of lines, discretizing in space variable by finite differences. We get a system of ODEs which we then solve by an embedded fourth-order Runge-Kutta Cash-Karp method with fifth-order error estimate. This choice of an ODE solver enables us to adaptively change the time step and thus keep the error resulting from the time discretization under a specified threshold.

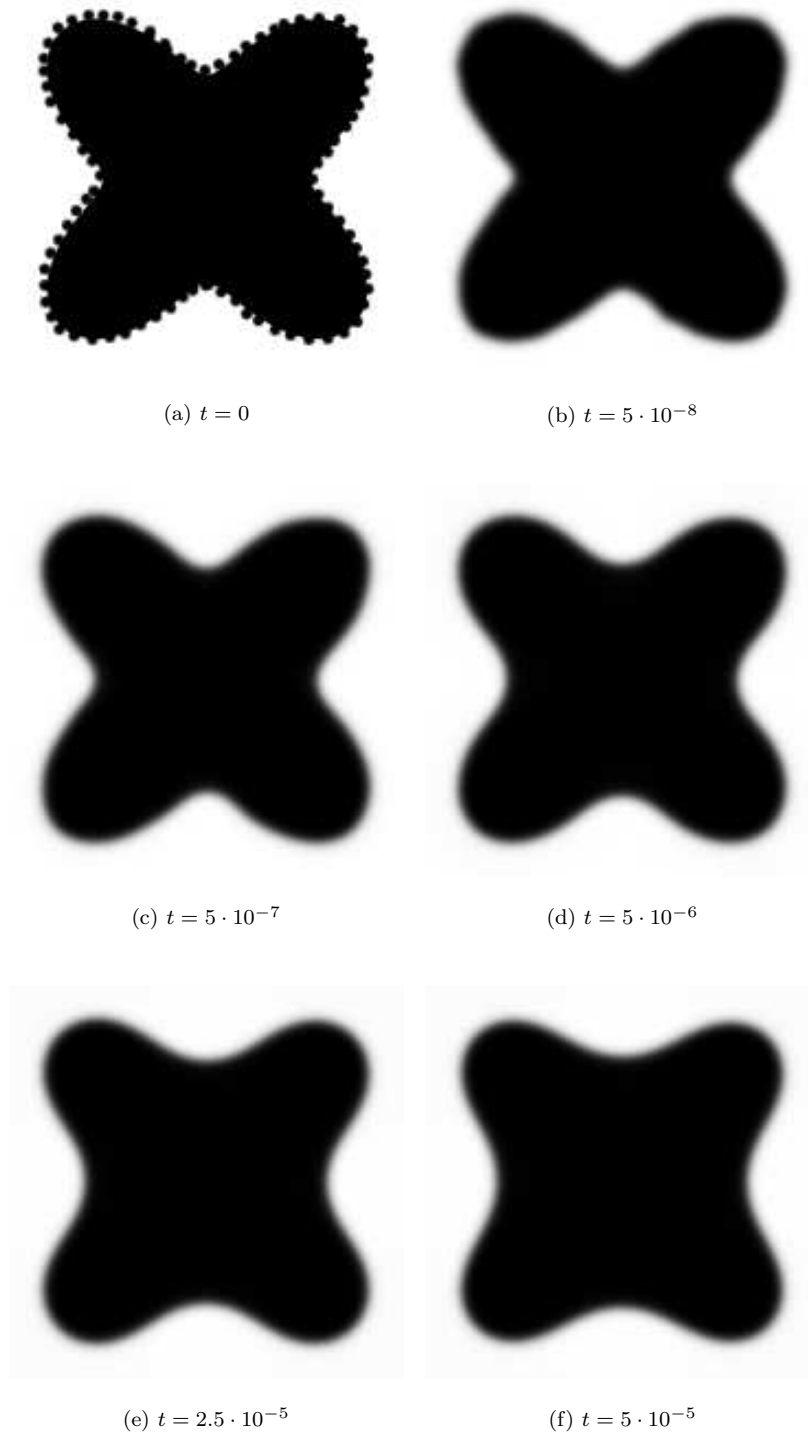


FIG. 6.1. *Shape recovery*: 180×180 pixels, $h = \xi = 1/179$



(a) $t = 0$



(b) $t = 2.5 \cdot 10^{-9}$



(c) $t = 5 \cdot 10^{-9}$



(d) $t = 10^{-8}$

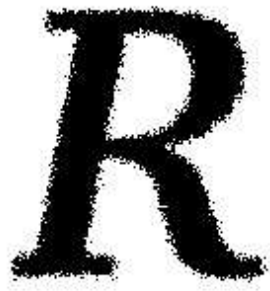


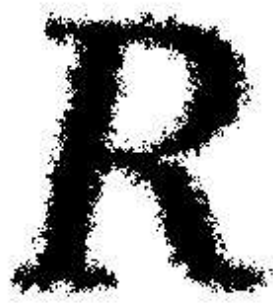
(e) $t = 2.5 \cdot 10^{-8}$



(f) $t = 5 \cdot 10^{-8}$

FIG. 6.2. *Shape recovery*: 200×200 pixels, $h = \xi = 1/199$

(a) $t = 0$ (b) $t = 2.5 \cdot 10^{-9}$ (c) $t = 5 \cdot 10^{-9}$ (d) $t = 10^{-8}$ (e) $t = 2.5 \cdot 10^{-8}$ (f) $t = 5 \cdot 10^{-8}$ FIG. 6.3. *Shape recovery: 20×200 pixels, $h = \xi = 1/199$*



(a) $t = 0$



(b) $t = 2.5 \cdot 10^{-9}$



(c) $t = 5 \cdot 10^{-9}$



(d) $t = 10^{-8}$



(e) $t = 2.5 \cdot 10^{-8}$



(f) $t = 5 \cdot 10^{-8}$

FIG. 6.4. *Shape recovery*: 20×200 pixels, $h = \xi = 1/199$

Then, we demonstrated experimentally that the proposed scheme converges with the first-order accuracy. In order to be able to easily run large computation, a parallel implementation is necessary and we shortly described such an implementation. The presented numerical scheme can be applied in the context of image processing for shape recovery of segmented images, we proposed such an algorithm and demonstrated its use on several images.

Acknowledgment. Partial support of the CTU Internal Research Grant No. CTU0410514 and of the project "Applied Mathematics in Technology and Physics" MSM 6840770010 of the Ministry of Education of the Czech Republic.

REFERENCES

- [1] J. W. BARRETT, J. F. BLOWEY AND H. GARCKE, Finite element approximation of the Cahn-Hilliard equation with degenerate mobility, *SIAM J. Numer. Anal.* **37**, (1999) 286 -318.
- [2] J. W. BARRETT, J. F. BLOWEY AND H. GARCKE, On fully practical finite element approximations of degenerate Cahn-Hilliard systems, *ESAIM Mathematical modelling and numerical analysis* **35**, (2001) 713 -748.
- [3] M. BENEŠ, Mathematical analysis of phase-field equations with numerically efficient coupling terms, *Interfaces and Free Boundaries* **3**, (2001) 201-221.
- [4] M. BENEŠ, Diffuse-Interface Treatment of the Anisotropic Mean-Curvature Flow, *Applications of Mathematics* **48**, (2003) 437-453.
- [5] M. BENEŠ, V. CHALUPECKÝ AND K. MIKULA, Geometrical image segmentation by the Allen-Cahn equation, *Applied Numerical Mathematics* **51**, (2004) 187-205.
- [6] M. BENEŠ AND K. MIKULA, Simulation of Anisotropic Motion by Mean Curvature - Comparison of Phase Field and Sharp Interface Approaches, *Acta Mathematica Universitatis Comenianae* **67**, (1998) 17-42.
- [7] J. W. CAHN, On spinodal decomposition, *Acta Met.* **9** (1961), 795-801.
- [8] J. W. CAHN AND J. E. HILLIARD, Free energy of a nonuniform system. I. Interfacial free energy, *J. Chem. Phys.* **28** (1958), 258-267.
- [9] J. W. CAHN AND J. E. HILLIARD, Free Energy of a Nonuniform System. III. Nucleation of a Two-Component Incompressible Fluid, *J. Chem. Phys.* **31** (1959), 688-699.
- [10] J. W. CAHN, J. E. HILLIARD AND A. NOVICK-COHEN, The Cahn-Hilliard equation with concentration dependent mobility: motion by minus the Laplacian of the mean curvature, *Eur. J. Appl. Math.* **7** (1996), 287-301.
- [11] I. C. DOLCETTA AND S. F. VITA, Area-preserving curve-shortening flows: from phase separation to image processing, *Interfaces and Free Boundaries* **4**, (2002) 325 -343.
- [12] C. M. ELLIOTT AND H. GARCKE, On the Cahn-Hilliard equation with degenerate mobility, *SIAM J. Math. Anal.* **27**, (1996) 404 -423.
- [13] X. FENG AND A. PROHL, Error analysis of a mixed finite element method for the Cahn-Hilliard equation, *Numer. Math.* **99**, (2004) 47 -84.
- [14] D. FURIHATA, A stable and conservative finite difference scheme for the Cahn-Hilliard equation, *Numer. Math.* **87**, (2001) 675-699.
- [15] J. C. JORGE AND B. BUJANDA, Numerical methods for evolutionary reaction-diffusion problems with nonlinear reaction terms, *J. Comput. Appl. Math.* **166**, (2004) 167-180.
- [16] J. KIM, K. K. KANG AND J. LOWENGRUB, Conservative multigrid methods for Cahn-Hilliard fluids, *J. Comput. Phys.* **193**, (2004) 511-543.
- [17] W. H. PRESS, B. P. FLANNERY, S. A. TEUKOLSKY AND W. T. VETTERLING, Numerical recipes in C, *Cambridge University Press*, (1992).